Investigation of defect structures in deformed and helium-irradiated refractory metals by positron annihilation



1993 J. Phys.: Condens. Matter 5 3987

(http://iopscience.iop.org/0953-8984/5/23/026)

J. Phys.: Condens. Matter 5 (1993) 3987–4006. Printed in the UK

# Investigation of defect structures in deformed and helium-irradiated refractory metals by positron annihilation

G Kögel, P Sperr, J Störmer and W Triftshäuser

Institut für Nukleare Festkörperphysik der Universität der Bundeswehr München, 8014 Neubiberg, Federal Republic of Germany

Received 8 June 1992, in final form 5 February 1993

**Abstract.** The defect structures in deformed and helium-irradiated refractory metals, vanadium, niobium and tantalum have been investigated by means of positron lifetime and Doppler broadening techniques. The evolution of the defects was studied by performing isochronal annealing programmes. In all three metals after deformation a single, well defined lifetime was observed which was 30 ps to 40 ps lower than that reported for vacancies. The recovery of the deformation-induced defects however, is remarkably different for niobium and tantalum as compared to vanadium. In helium-irradiated vanadium and niobium two distinctly different defect types were observed with characteristic lifetimes of about 190 ps and 375 ps, respectively. The longer lifetime is attributed to large helium bubbles. Both metals showed a similar behaviour in the annealing studies. All measured lifetime data are consistent with the simple trapping model. The influence of oxygen impurities and oxygen resorption during the isochronal annealing procedure is discussed.

## 1. Introduction

Recently the refractory metals of group Vb have received much interest. In particular, vanadium is a prominent candidate as a structural material for fusion devices because of lower activation and helium production under irradiation as compared to austenitic and ferritic steels [1, 2]. Positron annihilation is a standard tool for the investigation of defects caused by plastic deformation, radiation damage and helium segregation [3]. Whereas for the group VIb metals molybdenum and tungsten the annihilation characteristics of positrons for various defects and the thermal recovery of the defects have been investigated in great detail [4–6], only a small number of studies has been performed on the group Vb metals [7–11].

Besides the technological potential of vanadium, the entire BCC group Vb is also of considerable scientific interest, because of systematic similarities and discrepancies with the BCC group VIb of the periodic table. As far as positron annihilation is concerned, the *most striking trend is the trapping ability of positrons by thermally generated vacancies*, which is absent in the high temperature BCC phase of group IVb [12], weak in the group Vb [7] and very strong in group VIb [7]. This trapping occurs in spite of the fact that the binding energies of trapped positrons are expected to be of the same magnitude in all cases [9, 13]. Therefore an extrapolation of the annihilation characteristics of the group Vb metals from the well known values of the group VIb is quite uncertain and the present study was performed in order to provide more basic information for an investigation of helium segregation in V, Nb and Ta [14] by positron annihilation. In this paper we report results from simultaneous measurements of positron lifetimes and Doppler-broadened annihilation

0953-8984/93/233987+20$07.50  

lineshapes for isochronal annealing series of cold rolled V, Nb and Ta and of helium-irradiated V and Nb. The results and additional observations will be presented as completely as possible to facilitate a reanalysis in the light of better knowledge in the future, because our subsequent interpretation is impeded not only by the complicated microstructure of dislocations in BCC metals [15, 16], which implies a generally restricted understanding of defects in BCC metals, but even more by the considerable resorption of light interstitial impurities like C, N and O both from the ambient atmosphere and from insufficient vacuum conditions during the thermal treatments.

## 2. Details concerning the experiments

### *2.1. Samples and sample preparation*

Pure vanadium, niobium and tantalum foils of high quality (see table 1) and a thickness of 0.1 mm were cut into sheets 10 by 10 mm. The specimens were annealed at high temperature in ultra-high vacuum for about 30 min (see table 2), in order to produce a defect-free state for further investigations.

**Table 1.** Impurities ($\geqslant$ 10 ppm) of the vanadium, niobium and tantalum specimens as given by the supplier [46].

| Impurities ($\geqslant$ 10 ppm) | C | N | O | Al | Si | P | S | Fe | Ta |
|---|---|---|---|---|---|---|---|---|---|
| Vanadium | 20 | 15 | 60 | 40 | 130 | 46 | 10 | 51 | — |
| Niobium | 25 | — | 15 | — | 17 | — | — | — | 200 |
| Tantalum | 10 | — | — | — | — | — | — | — | — |

**Table 2.** Temperature and vacuum conditions during specimen preparation. The melting point temperatures are taken from [47].

| Specimen | Annealing temperature (K) | Vacuum condition ($10^{-6}$ Pa) | Melting point (K) |
|---|---|---|---|
| Vanadium | 1790 | $< 1$ | $2163 \pm 10$ |
| Niobium | 2170 | $< 1$ | $2741 \pm 10$ |
| Tantalum | 2270 | $< 1$ | 3269 |

The measured lifetimes of the defect-free state are $(126 \pm 2)$ ps for V, $(125 \pm 2)$ ps for Nb and $(123 \pm 2)$ ps for Ta. The values for Nb and Ta are in excellent agreement with those reported in [17].

In order to investigate the evolution of defect structures as a function of the deformation, the samples were cold rolled. One set of annealed V and Nb specimens was irradiated at the KFA Jülich with helium ions of variable energy ($E_{max} = 28$ MeV), in order to obtain a uniform damage profile. The irradiation temperature was about 325 K. Helium doses of 1000 ppm for V and 800 ppm for Nb were achieved. The helium injection procedure adopted was the same as that reported earlier [18]. The evolution of defect states was studied, performing isochronal annealing programs in small steps (about 20 K) from room temperature up to 1250 K in a high-temperature furnace. The vacuum during the annealing procedure was about $10^{-3}$ Pa. The annealing time was 30 min for each annealing step. The positron annihilation parameters were measured at room temperature.

### *2.2. Experimental set-up*

The positron sources ($^{22}$NaCl) were deposited on titanium foils of 1 mg cm$^{-2}$ thickness. The source strength was about 10 $\mu$Ci ($3.7 \times 10^5$ Bq) for the vanadium measurements and about 25 $\mu$Ci ($9.3 \times 10^5$ Bq) in the case of niobium and tantalum. For the lifetime measurements a conventional fast–slow coincidence set-up was used with $BaF_2$ scintillators in the case of the measurements of the vanadium samples and with fast plastic scintillators for the other two specimens. The time resolutions of the spectrometers with $^{22}$Na window settings were 220 ps (FWHM) and 200 ps (FWHM), respectively. Positron lifetime spectra were analysed by a non-linear least squares fitting procedure (modified version of POSITRONFIT [19]) with up to three lifetime components. About $6 \times 10^6$ events were accumulated for each lifetime spectrum.

In addition to the lifetime measurements the Doppler broadening of the 511 keV annihilation radiation was detected simultaneously. These measurements were performed using a high purity Ge detector with an intrinsic resolution of 1.2 keV (FWHM) at 497 keV. Thus, by combining positron lifetime and Doppler broadening measurements, information about the electron densities and the electron momentum distribution in the bulk and at defect sites could be obtained.

The stability of all systems (lifetime and Doppler spectrometers) was repeatedly controlled by measuring the resolution functions with well annealed stainless steel (SS316) samples.

## 3. Results and discussion

### *3.1. Defect structures in deformed vanadium*

Annealed vanadium samples were cold rolled to a successively greater thickness reduction. The measured annihilation characteristics are plotted in figures 1 and 2 against the degree of deformation, which is given in percent with respect to the undeformed sample.

The results obtained for the lifetimes $\tau$ and the corresponding intensities $I$ and for the Doppler lineshape parameter $I_v$ as function of the deformation are shown in figures 1 and 2, respectively. The $I_v$ parameter, whose definition is given in [20], was obtained by integration over a region of $\pm 1.5$ mrad (corresponding to $\pm 0.384$ keV) around the centroid of the 511 keV annihilation line. As can be seen from figure 2, the value of $I_v$ saturates at a deformation of about 11%.

The lifetime $\tau_2 = (166.8 \pm 2)$ ps represents the average value which was obtained from the analysis of the spectra at deformations above 6%. In subsequent analysis this value was kept fixed.

The lifetime $\tau_2$ is attributed to the annihilation of positrons at defects, mainly dislocations, which are created during the cold rolling procedure. It should be noted here too that in the isochronal annealing studies (see section 3.2) no change in the value of $\tau_2$ was observed.

The corresponding intensity $I_2$ is shown in the lower part of figure 1. Even at a very small deformation of 3.1%, the intensity $I_2$ is nearly 60%. Saturation is reached at a deformation of 11.2% in agreement with the behaviour of the $I_v$ parameter shown in figure 2. At saturation trapping (all positrons annihilate at defect sites) the mean lifetime $\bar{\tau}$ is equal to $\tau_2$. Our value of $\tau_2 = (166.8 \pm 2)$ ps is somewhat smaller than the value of 172 ps, which is given for 50% deformed vanadium in [21].

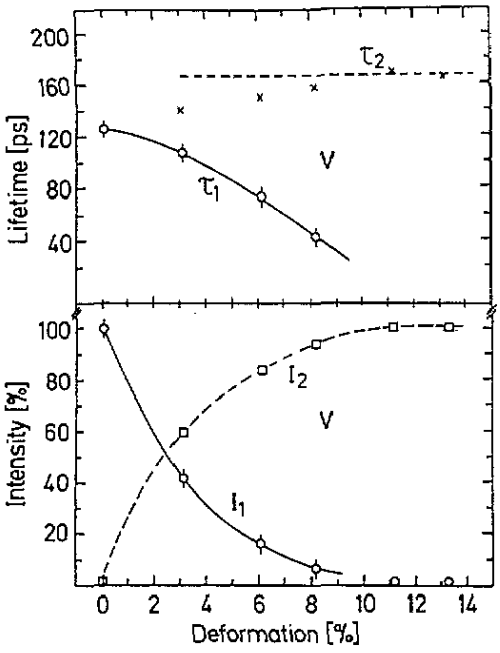


Figure 1. Positron lifetimes (upper part) and corresponding intensities for vanadium as function of the degree of deformation.

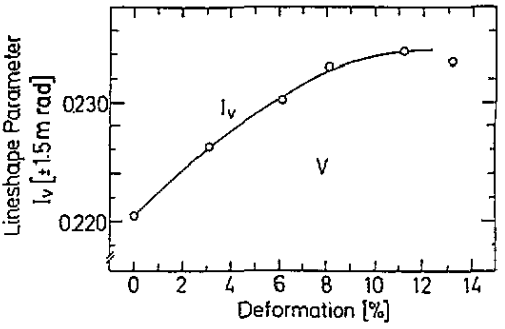


Figure 2. Lineshape parameter $I_v$ for vanadium as function of the deformation. The definition of $I_v$ is given in [20].

The occurrence of a quite early saturation trapping has also been observed in deformed iron [22] and the quoted mean lifetime of 167 ps at saturation is equal to the value we have found for vanadium.

As can be seen from figure 1, the lifetime $\tau_1$, which is the lifetime of the free positron, and the corresponding intensity $I_1$ decrease with increasing deformation and consequently tend to zero when all positrons are trapped at defects. The calculated value of the bulk lifetime $\tau_b$, according to the trapping model [3] is constant up to a deformation of about 8%.

### *3.2. Annealing study of deformed vanadium, niobium and tantalum*

An isochronal annealing programme was performed for cold rolled vanadium (deformation 13.3%), niobium (deformation 23%) and tantalum (deformation 15%). Good fits of the lifetime spectra were obtained only when two lifetimes $\tau_1$, $\tau_2$ and an additional 'source and surface term' $\tau_s$ of 400 to 700 ps with an intensity $I_s$ in the percent range were included. The extra source term is usually included in the analysis of positron lifetime spectra to account for the annihilation of positrons in the radioactive source and in the surface oxide of the specimen. Therefore $\tau_s$ and $I_s$ depend on both the source and the specimen. The source term was derived separately for the frequently measured reference samples (see section 2.2). Within the statistical error limits the source term was constant for the reference samples. In all Ta and Nb samples which were subjected to thermal treatment, however, $I_s$ exhibited a marked, consistent dependence on the annealing temperature. We believe that this consistent trend is related to the resorption of oxygen by the samples. This resorption may influence the annealing behaviour as well, therefore we first discuss the temperature dependence of the source and surface term.

*3.2.1. Dependence of the source and surface term on the annealing temperature and on the resorption of oxygen.* The evolution of $I_s$ is shown in figure 3 for all specimens which exhibited this trend. For the vanadium specimens this trend could not be observed. In helium-irradiated vanadium it was impossible to separate the source contribution $\tau_s$ from the longest lifetime $\tau_3$ (see figure 13). In deformed vanadium the recovery was completed at an annealing temperature ($T_a$) of about 700 K. As can be seen from figure 3, up to this temperature $I_s$ remains more or less constant.

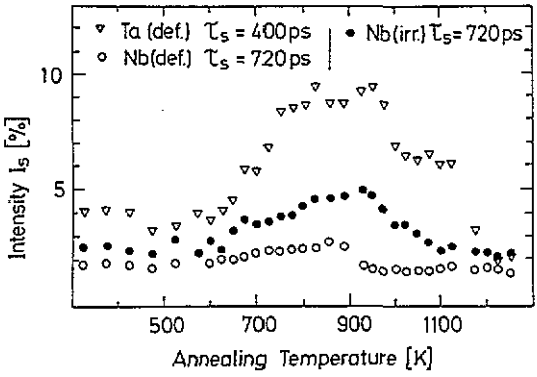


**Figure 3.** Intensity $I_s$ of the 'source and surface term' $\tau_s$ for Ta and Nb specimens as function of the annealing temperature. For details see section 3.2.1.

From the surprisingly good correlation of the independently determined evolution $\tau_s(T_a)$ we conclude a common feature: the high value of $\tau_s = 720$ ps for the niobium samples is typical for positron lifetimes in defective oxides [23], whereas the value of $\tau_s = 400$ ps observed in tantalum could be attributed to large vacancy clusters as well (see table 3). However, this value for $\tau_s$ was also observed in the undeformed tantalum.

**Table 3.** Positron lifetimes (in ps) for vanadium, niobium and tantalum at various defective states. The numbers in the brackets indicate the relevant references, the star means values obtained in this work.

| Defective state | V | Nb | Ta |
|---|---|---|---|
| Deformed | 167 [*] | 170 [*] | 176 [*] |
| Vacancy | 191 [38] | 210 [9] | 203 [9] |
| Electron-irradiated annealed at 300 K | | 450 [9] | 400 [9] |
| Helium-irradiated $\tau_2$ as-irradiated | 190 [*] | 187 [*] | — |
| $\tau_3$ as-irradiated | 370 [*] | 380 [*] | — |
| Neutron-irradiated | 452 [48] | 477 [48] | — |

A similar behaviour is reported from an annealing study of tantalum with a deformation of 50% [21], where a long lifetime of about 600 ps was observed only between 650 and 1100 K with a maximum intensity of 5% at 850 K. The authors of [21] attribute this lifetime to large vacancy clusters which grow between 650 K and 800 K and subsequently dissolve at

higher annealing temperatures. Typically, the condensation of vacancies into larger clusters causes a gradual increase of the largest resolved lifetime and not the abrupt appearance of an additional much longer lifetime. This general behaviour was indeed observed in electron irradiated tantalum as well [9]. Therefore we believe that our results (see figure 3) as well as the results of [21] are more indicative of the continuous growth and subsequent dissolution of an oxygen-enriched surface layer than of the formation and subsequent dissolution of large vacancy clusters.

In order to check this conclusion, a brief discussion of the available results for the resorption of oxygen in group Vb metals is given below. For each metal only a restricted amount of information is available. Therefore the results for different metals had to be combined by invoking the well known chemical similarity of the group Vb metals. As a consequence, only qualitative estimates can be deduced. Besides oxygen we also expect the uptake of hydrogen, carbon and nitrogen. However, the surface oxide is an efficient barrier for hydrogen, whereas the involved activation energies for carbon and nitrogen are systematically higher when compared to the values for oxygen [24]. Therefore oxygen is expected to cause the major contamination during the experiments. Oxygen resorption only becomes relevant for the recovery of the defects in the bulk of the specimens, if

(i) the oxygen atom is chemisorbed in the surface oxide,
(ii) the oxygen is dissolved as an interstitial, and
(iii) the interstitial diffuses into the bulk of the specimen.

In air at 300 K step (i) follows a logarithmic time law which is, for oxide layers below a thickness of 1 nm, identical for Ta and Nb [25]. Within 1000 min the oxide layer of Nb, which was cleaned in ultra-high vacuum, grows to about 1.5 nm [26]. Under vacuum conditions the logarithmic time law is valid up to about 800 K [27]. At higher temperatures in high vacuum the resorption of oxygen becomes linear with exposure time and with the partial pressure of oxygen [28]. The temperature dependence, which is rather complex, was investigated for Ta in the temperature range from 970 K to 1340 K [28]. From the published data, we have determined that the additional growth of the oxide surface layer, during 20 min of annealing at elevated temperatures in a vacuum better than $10^{-3}$ Pa, is negligible below 800 K, corresponds to 0.5 nm at 1000 K and to 1 nm in the range from 1050 K to 1255 K.

Step (ii) is rather complex, because the oxide layer grows inhomogeneously and because 'fingers' of suboxide can penetrate the bulk metal even at 300 K [26, 29]. Investigations of the dissolution of a compact layer of $Nb_2O_5$ on Nb in the temperature range from 600 K to 640 K are given in [29]. According to these results the dissolution of interstitial oxygen from the surface oxide is negligible from 300 K up to annealing temperatures of 550 K. At higher annealing temperatures, according to [29], at least 1 nm of the oxide layer will always be dissolved.

Finally, in step (iii) the interstitial oxygen has to diffuse into the bulk of the metal. For Nb and Ta, the same diffusion constant $D \approx 0.02 \exp(-13\,500/T)$ cm$^2$ s$^{-1}$ is reported [24]. Due to the rapid increase of $D$ as a function of the annealing temperature, it is sufficient to consider for isochronal annealing only the diffusions in the last temperature treatment. If we take the mean square displacement $\bar{x}$ of the interstitial oxygen as a measure for the thickness of the zone enriched with dissolved interstitial oxygen, we obtain for 20 min of annealing time the relation: $\bar{x}(T) = 5 \times 10^7 \exp(-6750/T)$ nm.

Obviously the interstitial oxygen is continuously distributed in the bulk of the specimens, if $2\bar{x}$ exceeds the thickness of the specimen. This condition is fulfilled for $T \geqslant 1000$ K. In figure 4 we have plotted the pertinent quantities for the resorption of interstitial oxygen in

our Nb and Ta specimens, as estimated from the data compilation given above, against the annealing temperature for our experimental conditions as described in section 2.

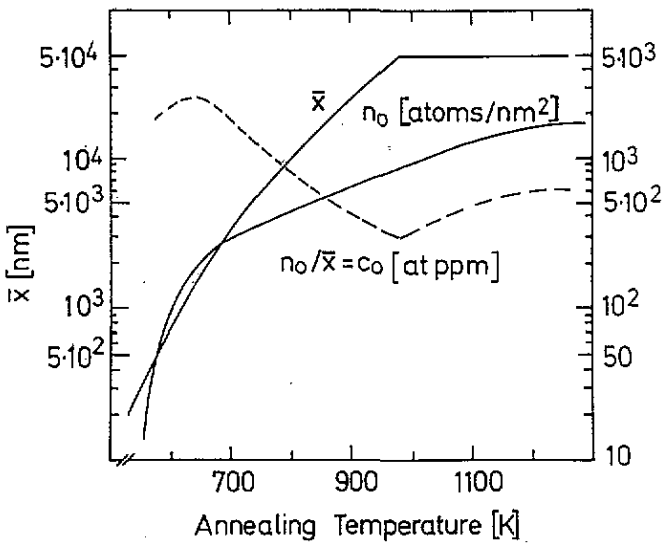


**Figure 4.** Mean square displacement $\bar{x}$ and number $n_0$ of the resorbed interstitial oxygen impurities in Ta and Nb as function of the annealing temperature. The right hand scale applies to $n_0$ and to $c_0 = n_0/\bar{x}$ (broken line), further details are given in section 3.2.1.

Here $n_0$ denotes the number of the resorbed interstitial oxygen impurities per surface area unit ($nm^2$) and $c_0 = n_0/\bar{x}$ is the average concentration (at ppm) of interstitial oxygen in the subsurface oxygen enriched layer with the width $\bar{x}$. The general trends observed in the measured intensities $I_s$ of the source and surface contribution (see figure 3) and the characteristics of the oxygen resorption (see figure 4) are correlated consistently. Below 600 K the amount $n_0$ of resorbed oxygen and the value of $\bar{x}$ are too small for measurable effects. The abrupt increase of $I_s$ around 650 K is correlated with the maximum in the concentration of interstitial oxygen $c_0$, which occurs at a layer thickness of about 2 $\mu$m. The decrease of $I_s$ finally is correlated with the minimum in $c_0$ and with the extension of the oxygen enriched layer into the bulk of the specimen at 1000 K.

*3.2.2. The evolution of defects in deformed vanadium, niobium and tantalum as a function of the annealing temperature.* For all three metals, the longer lifetime $\tau_2$ remains nearly constant up to the highest annealing temperatures (see figure 6). The absolute values of $\tau_2$ in all cases are considerably shorter (about 30 to 40 ps) than those reported for lifetimes in single vacancies (see table 3). Therefore positrons are trapped and annihilate preferentially at dislocations and not at isolated vacancies, which could also be introduced by the deformation. This behaviour is reported for many FCC metals (see e.g. [30] and references therein). The observed relative magnitude of the lifetimes for annihilations in the bulk, at dislocations and at vacancies is consistent with the results of a recent theoretical investigation [30] for the FCC metals Cu and Al. According to [30] the most probable annihilation sites are vacancies in the core of the dislocations or in stacking faults. The validity of the simple two-stage trapping model [3] is proven (in figure 8) by comparing the bulk lifetime $\tau_b$ (see section 3.1) and the quantity $\tau^* = (I_1/\tau_1 + I_2/\tau_2)^{-1}$ as calculated from

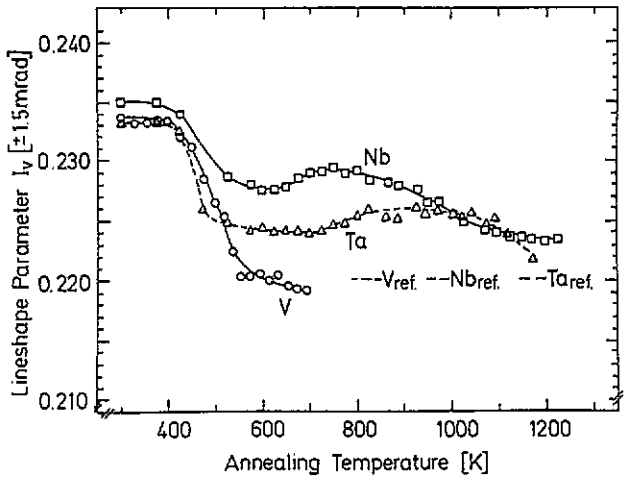


**Figure 5.** Lineshape parameter $I_v$ for deformed V, Nb and Ta specimens as a function of the annealing temperature. The reference values ($--X_{ref.}$) for the well-annealed samples are given in the figure. The curves are only to guide the eye.

the data of figures 6 and 7. Data sets with an intensity $I_1 < 10\%$ were omitted in figure 8. As required by the two-stage trapping model we obtain $\tau^* = \tau_b$. Besides this, the recovery in vanadium differs markedly from that in niobium and tantalum. Whereas in the case of vanadium almost complete recovery occurs in a single stage from 400 K to 550 K, which is the same for the lifetime and Doppler-broadening data (see figures 5 and 6), the lifetime data for tantalum and niobium show a weak monotonic recovery beginning at 500 K which is not completed at the highest annealing temperatures investigated (see figures 5 and 6). In contrast to this, the $I_v$-parameter (see figure 5) shows for niobium and tantalum a quite different dependence on the annealing temperature including stages of fast recovery and a region of increase with increasing annealing temperature. This retrograde evolution of $I_v$ is weakly correlated with the trend of the source intensity $I_s$ (see figure 3). However, the direct contribution to $I_v$ of positrons which annihilate in the surface layer explains only a few percent of the anomaly. Therefore a rearrangement in the microstructure of the defects must be assumed which alters the $I_v$ parameter without changing the positron lifetime. In order to clarify this speculation, in figures 9 to 11 the $I_v$ parameter and the mean lifetime $\bar{\tau} = I_1\tau_1 + I_2\tau_2$ are correlated for all three metals. The mean lifetime $\bar{\tau}$ is less affected by minor errors in the fitting procedure than the individual lifetimes and the concentrations. Moreover, as long as detrapping from defects is neglected, from the trapping model for an arbitrary number $(m-1)$ of different defects with specific trapping rate $\kappa_i$, concentration $c_i$, defect specific lifetime $\tau_i$ and lineshape parameter $I_{v,i}$ respectively, the general relation

$$(I_v - I_{v,b}) = (\bar{\tau} - \tau_b)\left[\sum_{i=2}^{m} \kappa_i c_i (I_{v,i} - I_{v,b})\right] \Big/ \left[\sum_{i=2}^{m} \kappa_i c_i (\tau_i - \tau_b)\right]$$

is obtained. Here $I_{v,b}$ and $\tau_b$ denote the lineshape parameter and the lifetime in the well annealed specimen, respectively. Thus the correlation $I_v$ versus $\bar{\tau}$ for the evolution of a defect ensemble will be a straight line including the point $I_{v,b}(\tau_b)$ if only one kind of defect is present, or if the relative concentrations $c_i$ are in constant proportion during the evolution. Hence from figure 9 we can conclude that in vanadium the dislocations are disappearing, since the values for deformed and annealed vanadium fall on a straight line.

In niobium and tantalum the correlation $I_v(\bar{\tau})$ (figures 10 and 11) differs considerably from a straight line. Obviously the whole evolution can be divided into three different stages.

In stage 1 (annealing temperatures for tantalum up to about 550 K) there is a rapid variation of $I_v$ but only a minor recovery in $\bar{\tau}$. In stage 2 (550 K to 750 K for niobium and 550 K to 925 K for tantalum) there is a weak increase in $I_v$ and a strong decrease of $\bar{\tau}$. Finally in stage 3 (annealing temperatures above 750 K for niobium and above 925 K for tantalum) there is a linear correlation of $I_v(T_a) - I_{v,b}$ versus $\bar{\tau}(T_a) - \tau_b$, indicating the continuous recovery of one kind of defect in this stage. It is known that in BCC metals many different microscopic arrangements of dislocations, stacking faults and point defects are possible after plastic deformation [15]. In stage 1 of the recovery of niobium and tantalum (see figures 10 and 11) no resorption of oxygen in the volume of the specimen is expected (see section 3.2.1). Furthermore, in stage 1 the intensity $I_2$ for the annihilation at defects remains constant. Therefore the recovery in stage 1 of niobium and tantalum must be due to an internal conversion, or relaxation, of the defective regions which only affects the defect specific lineshape parameter $I_{v,2}$ without any effect on the defect specific lifetime $\tau_2$. Without a detailed theoretical investigation no definite conclusions are possible on the nature of this relaxation. From the results of [30], however, it seems plausible that the relative numbers of vacancies in the dislocation cores and in stacking faults are changed in this relaxation process. No substantial reduction in the defect concentration takes place in stage 1 of niobium and tantalum, in sharp contrast to the case of vanadium, where the defects disappear without any detectable change in the characteristic lineshape parameter $I_{v,2}$.

In stage 2 of niobium and tantalum the intensity $I_2$ of the lifetime $\tau_2$ decreases continuously (see figure 7). Therefore defects disappear in stage 2. However, the observed lineshape parameter remains constant or even increases. Therefore the momentum distribution of the electrons changes in stage 2 at the annihilation sites of the positron (see figures 5, 10 and 11).

An increasing decoration of the defects by oxygen is the most convincing interpretation, since the formation of defects with a larger free volume is excluded by the observed invariance of $\tau_2$ and since the temperature range of stage 2 coincides with the range where the resorption of oxygen becomes important (see figures 3 and 4).

Finally in stage 3, the correlation $I_v(\bar{\tau})$ indicates a recovery process, where the specific annihilation characteristics of the defects remain unaltered, for instance because the decoration by interstitial oxygen is saturated.

The present results are in complete agreement with the lifetime data reported in [21] for V, Nb and Ta, each deformed by 50%. In the case of Ta, the authors of [21] propose a different interpretation for a weak component $\tau_3 \approx 600$ ps with intensities below 5% (see section 3.2.1). The results do not agree with those reported in [10] for deformed niobium. However, in the latter work, specimens with up to 5000 ppm of impurities were used. Because of the high sensitivity of the recovery to the impurity concentration, the disagreement is most probably due to the different purity of the specimens. On the other hand we do not expect, in our specimens, a large influence of the impurities on the recovery process itself, because the interaction energy of interstitials and dislocations in BCC metals is $< 1$ eV [15]. Therefore pinning of dislocations, by a small concentration of interstitials, should be very weak at annealing temperatures above 600 K, where the resorption of oxygen becomes effective. Only for high impurity concentrations may there be a strong collective effect, which is probably seen in our results for niobium at annealing temperatures in excess of 1100 K (see figures 6 and 7).

*3.3. The evolution of defects in helium-irradiated vanadium and niobium as function of the annealing temperature*

The helium irradiated vanadium and niobium samples were always annealed together with the deformed specimens. In figure 12 the results of the Doppler-broadening measurements are presented. When compared to the results of the deformed specimens (see figure 5), the evolution of $I_v$ as a function of the annealing temperature shows a number of remarkable differences:

(i) in the as-irradiated state, the difference of $I_v$ to the bulk value is about twice that observed in the deformed samples,

(ii) the onset of the recovery is shifted to higher temperatures,

(iii) instead of the marked antirecovery stage observed in deformed Nb (see figure 5) there is only a weak shoulder around 950 K in the helium-irradiated specimen.

Finally the recovery in V is not completed even at an annealing temperature of 900 K. Even more drastic differences are visible in the results of the lifetime measurements, which are shown in figure 13. For annealing temperatures above 750 K in vanadium and 900 K in niobium, good fits were obtained only when three unconstrained lifetimes were allowed in addition to the source term as discussed in section 3.2. Two different groups of defects can be clearly distinguished due to the lifetimes $\tau_2$ and $\tau_3$ in the as-irradiated state. The longer lifetime $\tau_3 \approx 375$ ps for both irradiated metals indicates the existence of large vacancy clusters (cf table 3), whereas the shorter lifetime $\tau_2$ with initial values of 195 ps for V and 186 ps for Nb is considerably larger when compared to the values reported in section 3.2 for the deformed specimens. In the case of Nb the initial value of $\tau_2$ is considerably shorter when compared to the value reported for vacancies (see table 3). Therefore the smaller defects introduced by the irradiation may be vacancies decorated with helium or dislocation loops where the annihilation sites of the positrons are somewhat expanded due to the presence of helium or a mixture of both kinds of defects. The high initial value of $I_3$ (approx. 25%) indicates that about one quarter of the defects, which survive at the irradiation temperature of 325 K, form large clusters already during the irradiation. The annealing behaviour of the smaller defects is quite similar to that observed for the deformed specimens (see figures 6 and 7). While $\tau_2$ remains constant, the intensity $I_2$ and thus the concentration of the smaller defects decreases continuously for temperatures above 600 K in Nb and above 725 K in V, respectively. Compared to the deformed specimens, the onset of the recovery is shifted by 50 K and 275 K in the helium-irradiated Nb and V, respectively. This indicates a stabilization of the smaller defects due to helium decoration.

Fortunately, for annealing temperatures above 750 K in vanadium and above 900 K in niobium, the lifetime $\tau_1$ and the intensity $I_1$ could be measured. Therefore we can derive the trapping rates $K_2$ and $K_3$ for trapping at the smaller and larger defects from the trapping model:

$$K_i = I_i(1/\tau_1 - 1/\tau_i) \qquad \text{with } i = 2, 3.$$

In order to reduce the scatter introduced by the large fluctuations of $\tau_1$ (see figure 13), this lifetime has been approximated by the best fitting straight line in the evaluation of $K_2$ and $K_3$. The results given in figure 14 clearly show that $K_2$ and $K_3$ are continuously decreasing. Thus the maximum in $I_3$, which is observed for niobium just at the temperature of the minimum in $\tau_3$, is an incidental artifact of the positron annihilation measurement.

In the as-irradiated state 25% of the positrons annihilate from large vacancy clusters with a lifetime $\tau_3 \approx 375$ ps. These clusters may contain helium. The formation of large

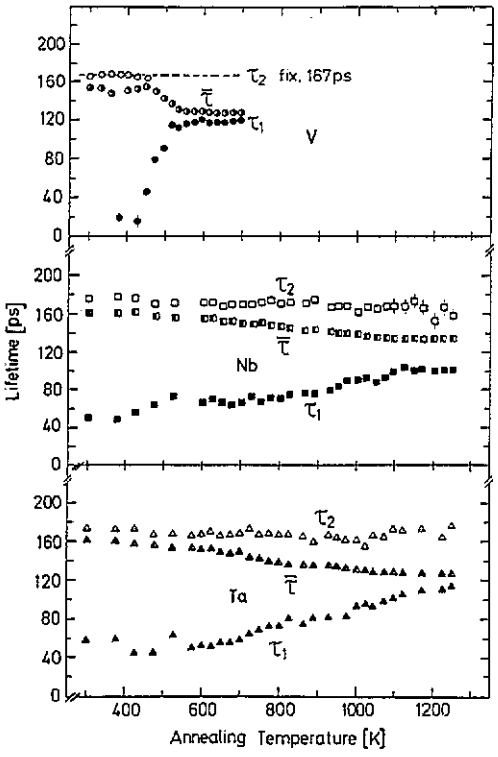


**Figure 6.** Positron lifetimes $\tau$ for deformed V, Nb and Ta specimens as a function of the annealing temperature.

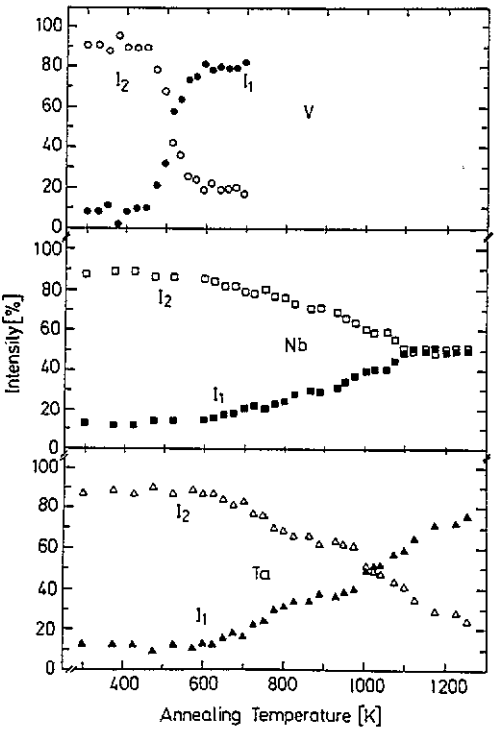


**Figure 7.** Intensities $I_1$ and $I_2$ of the corresponding lifetimes for deformed V, Nb and Ta specimens as function of the annealing temperature.

clusters even during irradiation has also been observed in neutron-irradiated Nb [31] (see also [48]). Also by transmission electron microscopy, bubbles with diameters of many nm have been observed in helium-irradiated vanadium and niobium after annealing at 1120 K [32].

The most surprising feature is the trend of $\tau_3$ as a function of the annealing temperature (see figure 13). Usually, the lifetime of positrons trapped in voids or gas-filled bubbles increases continuously as a function of the annealing temperature [33]. In the case of niobium this general trend is clearly visible. However, there is an intermediate temperature range with a substantial decrease of $\tau_3$, ranging from about 700 K to 900 K in V and from about 900 K to 1100 K in Nb. Such a trend in the largest resolved lifetime has already been observed in helium-irradiated nickel [34] and helium-irradiated molybdenum [35].

Various effects may contribute to the variation of $\tau_3$. All observations can be explained within the standard model for the evolution of positron annihilation characteristics in helium bubbles (see [36] for a recent review). Within this model the decrease of $\tau_3$ is attributed to the absorption of interstitial helium, whereas the subsequent increase of $\tau_3$ is explained by the pressure-induced growth of the bubbles, and the continuous decrease of $K_3$ is explained by coalescence of the bubbles. This interpretation is discussed in sections 3.3.1 and 3.3.2 for niobium and vanadium, respectively. Other possible effects are considered in section 3.3.3.

*3.3.1. Niobium.* For sufficiently large ($\geqslant$ 1 nm) bubbles, the positron lifetime depends only on the helium density $n_{He}$. By comprehensive experimental [37] and theoretical [38]

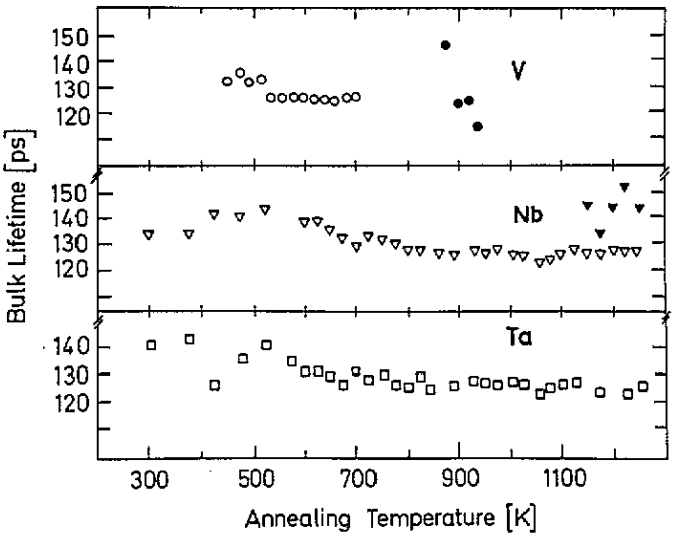


**Figure 8.** Calculated bulk lifetime $\tau^*$ for V, Nb and Ta as function of the annealing temperature. Open and closed symbols refer to data from deformed and helium-irradiated specimens, respectively.

investigations this dependence has been established as $\tau = 500 - 23.5 n_{He}(10^{22}\ cm^{-3})$ ps for helium bubbles in aluminium with bubble radii $\geqslant 1$ nm. The application of this relation to other metals has been discussed recently [36]. A value of 500 ps is generally accepted as the positron lifetime in surface states of large voids irrespective of the metal. In table 4 the resulting values of $n_{He}$ as calculated from $\tau_3$ in figure 13 are given together with the internal helium pressure $p_{He}$ as calculated from the equation of state for the respective annealing temperatures. In the evaluation of $p_{He}$ the nomogram published in [39] has been used. It is clearly seen that the helium density in the bubbles increases considerably during the annealing treatments between 900 and 1100 K. We believe that this increase is due to the absorption of interstitial helium which was released from the smaller defects. Helium desorption experiments have not been performed for niobium so far. However, in molybdenum the release of helium from monovacancies decorated with a single helium atom was observed at a temperature of 1170 K [40]. From this temperature and from the ratio of the calculated values for the dissociation energy $E_d$ of the monovacancy-helium complex [41], which are $E_d = 3.18$ eV (Nb) and 4.09 eV (Mo), we predict the release of helium from monovacancies to occur at 990 K in niobium. A considerably fraction of the released helium atoms will eventually be absorbed in the large clusters. The same interpretation has been given for a corresponding drop in the longest resolved lifetime in the case of a helium-implanted nickel [34] and helium-implanted molybdenum [35].

Furthermore, the mean bubble radius was evaluated from the measured values of the total trapping rate $K_3$ (see figure 13). In the case of aluminium, the specific trapping rate $\mu_B$ depends on the bubble radius $r_B$ (nm) according to

$$\mu_B = (1/(Ar_B) + 1/(Br_B^2))^{-1}$$

with $A = 9.07 \times 10^{16}\ nm^{-1}\ s^{-1}$ and $B = 3.30 \times 10^{16}\ nm^{-2}\ s^{-1}$ [37]. The application to other metals has also been discussed in [36]. In the case of niobium and vanadium it seems reasonable, because the specific trapping rate at monovacancies is similar, i.e. $10^{15}\ s^{-1}$ for

**Table 4.** Characteristic parameters of helium bubbles in niobium as derived in section 3.3.1. The acronyms are explained there.

| Annealing temperature (K) | $c_{He}$ (ppm) | $n_{He}$ ($10^{22}$ cm$^{-3}$) | $r_B$ (nm) | $p_{He}$ (GPa) | $p_{crit}$ (GPa) |
|---|---|---|---|---|---|
| 900 | 348 | 4.3 | 2.6 | 1.1 | 4.3 |
| 950 | 445 | 5.0 | 3.0 | 1.7 | 3.8 |
| 1000 | 542 | 5.7 | 3.4 | 2.1 | 3.3 |
| 1050 | 616 | 6.9 | 3.5 | 3.5 | 3.2 |
| 1100 | 655 | 8.1 | 3.6 | 5.0 | 3.1 |
| 1150 | 693 | 7.0 | 4.8 | 4.1 | 2.4 |
| 1200 | 723 | 5.4 | 6.5 | 2.1 | 1.8 |
| 1250 | 739 | 4.3 | 8.6 | 1.4 | 1.3 |

niobium and vanadium [7] and $5\times10^{14}$ s$^{-1}$ for Al [36], and because the positron diffusivities are similar, i.e. 1.6 cm$^2$ s$^{-1}$ for Al [36] and 1.4 cm$^2$ s$^{-1}$ for vanadium and 0.85 cm$^2$ s$^{-1}$ for niobium [42].

Since $K_3$ is related to the bubble concentration $c_B$ according to $K_3 = \mu_B c_B$ and since the total helium inventory in the bubbles, $c_{He}$, is $c_{He} = 4\pi c_B n_{He} r_B^3/3$ the mean bubble radius $r_B$ is related to $K_3$ (GHz), $c_{He}$ (at ppm) and $n_{He}$ ($\times10^{22}$ cm$^{-3}$) by the equation $r_B$ (nm) $= -1.37 + [1.88 + 2.16 c_{He}/(K_3 n_{He})]^{1/2}$. In the equation for $r_B$, the total helium inventory in the bubbles is unknown, though an upper limit for $c_{He}$ is provided by the implanted amount of helium. According to the interpretation given above for the increase of $n_{He}$, we have assumed that the amount of helium retained by the smaller defects is proportional to the concentration of these defects, i.e. to $K_2$. This assumption is strongly suggested by the striking stability of $\tau_2$ as a function of the annealing temperature, which indicates the annealing of the defects without major structural changes. The proportionality factor has been derived from the variation of $n_{He}$ between 900 and 1100 K under the assumption that the bubble growth up to the minimum of $\tau_3$ (i.e. up to an annealing temperature of 1100 K) is only due to bubble coalescence. Then from $K_2$ the values of $c_{He}$, and in turn the bubble radii $r_B$, were calculated (see table 4).

Up to an annealing temperature of 1100 K the bubble radius increases only gradually, whereas the internal pressure $p_{He}$ increases rapidly to a maximal value of 5 GPa. For higher annealing temperatures $r_B$ increases progressively whereas $p_{He}$ decreases continuously. The entire evolution suggests that at 1100 K, i.e. at the minimum of $\tau_3$, the internal pressure in the bubbles has reached the mechanical stability limit [39], and that for higher annealing temperatures the helium density in the bubbles decreases because of pressure induced loop punching [39]. To check this hypothesis, we have calculated the critical pressure $p_{crit}$ for loop punching from the relation [39] $p_{crit} = (2\gamma + 0.5Gb/(1-\nu))/r_B$. Here $\gamma$, $G$, $b$ and $\nu$ denote the surface energy, the shear modulus, the Burgers vector of the emitted loops and Poisson's number, respectively. Because the relation was derived for isotropic solids, a suitable average value $\bar{G}$ has to be used for the cubic crystal, where $G$ is anisotropic. We have calculated $\bar{G}$ from the elastic constants according to $\bar{G} = (C_{11} - C_{12} + 2C_{44})/4$. The values for $p_{crit}$ in table 4 have been obtained with $\gamma = 1$ N m$^{-1}$ [32], the Burgers vector $a/2\langle111\rangle$ and with elastic constants as given for the respective annealing temperatures in [43]. As may be seen from table 4, the internal pressure $p_{He}$ exceeds the critical pressure $p_{crit}$ for loop punching for annealing temperatures above 1100 K. This general trend seems to be insensitive to small variations in the functional dependences of $\tau_3$ on $n_{He}$ or $\mu_B$ on $r_B$. Possibly the expected trapping of positrons at the emitted dislocation loops is visible in the changing slope of $K_2(T)$ for annealing temperatures above 1050 K. It should be

noted that the increase of $r_B$ (see table 4) depends mainly on the coalescence of bubbles [32] due to their diffusive motion. However, the evolution of $\tau_3$ cannot be understood only as a consequence of bubble coalescence, because the mean helium density in the bubbles remains unchanged by this.

The evolution of helium bubbles in helium-irradiated molybdenum, as reported in [35] exhibits a characteristic difference. In molybdenum only two lifetimes have been resolved [35]. The longer lifetime, $\tau_2$, decreases from about 470 ps at 1100 K to 375 ps at 1300 K and remains unchanged up to the highest annealing temperatures of 1600 K [35]. The decrease in $\tau_2$ is also explained by the resorption of helium which was released from smaller defects [35]. By similar arguments as used above, a helium density $n_{He} = 5.3 \times 10^{22}$ cm$^{-3}$, an internal pressure $p_{He} = 1.9$ GPa and a bubble radius $r_B = 4.8$ nm are derived for the bubbles above 1300 K. For this bubble radius we obtain from the elastic constants of molybdenum [43] and with a surface energy $\gamma = 2.39$ N m$^{-1}$ [35] a critical pressure for loop punching $p_{crit} = 5.3$ GPa in molybdenum at 1300 K. Therefore, the striking difference in the evolution of $\tau_3$ between niobium and molybdenum is obviously due to the fact that the internal pressure $p_{He}$ in the case of molybdenum always stays below the critical value required for loop punching.

*3.3.2. Vanadium.* Here the trapping rates $K_2$ and $K_3$ for corresponding states in the evolution of $\tau_3$ are considerably larger than in the case of niobium. The difference is much larger as the difference in the helium implantation doses (see figures 13 and 14). Therefore the trapping rates at the maximum of $\tau_3$ (around 700 K) cannot be determined since $\tau_1$ and $I_1$ are too small. Hence the analysis of the bubble parameters is less complete than in the case of niobium.

The helium density in the helium bubbles, $n_{He}$, increases from $5.3 \times 10^{22}$ cm$^{-3}$ at 700 K to $9.1 \times 10^{22}$ cm$^{-3}$ at 900 K, corresponding to an internal pressure of 6.0 GPa at 900 K. As in the case of niobium, this increase is attributed to the incorporation of interstitial helium which was released from smaller defects. Helium desorption experiments for vanadium [44] have shown that the release of implanted helium starts around 600 K and follows an Arrhenius law for higher temperatures. The helium inventory in the helium bubbles can only be estimated from the analogy with niobium. If we assume that at 900 K the bubbles contain the same fraction of the total amount of helium (82%) as in the case of niobium at the minimum of $\tau_3$ (see table 4), than the mean average bubble radius $r_B = 2.7$ nm and the critical pressure $p_{crit} = 4.2$ GPa are obtained by the procedures as described in section 3.3.1. From these numbers we also expect an increase of $\tau_3$ because of pressure-induced bubble growth for vanadium at higher annealing temperatures.

*3.3.3. Discussion of alternative interpretations.* Various effects may contribute to the decrease or increase of $\tau_3$. Any possible effect must contribute a corresponding variation of the free volume of the defects. In addition to the incorporation of interstitial helium the reduction of the free volume could be achieved by incorporation of

(i) self-interstitials or interstitial loops,
(ii) interstitial oxygen,
(iii) the evaporation of vacancies,
(iv) a preferential annealing of the largest vacancy clusters,
(v) the generation of smaller clusters with an unresolved lifetime $\tau_4$, with $\tau_2 < \tau_4 < \tau_3$, from the continuously disappearing small defects.

Possibility (i) is ruled out because isolated self-interstitials become mobile at much lower temperatures [9] and because the concentration of vacancies and interstitial loops is expected to be similar [45].

The decoration by oxygen (possibility (ii)) is improbable, because in Nb the lifetime and the $I_v$ parameter are both known to be increased by the decoration of voids with oxygen [31]. The evaporation of vacancies (possibility (iii)) and a preferential recovery of larger clusters are both unlikely because these effects should be even more pronounced at elevated temperatures. Thus the lifetime $\tau_3$ should continue to decrease in contrast to the behaviour observed as shown in figure 13. Finally the generation of additional defects (possibility (v)) is ruled out by the monotonic decrease of the trapping rate $K_3$ in the temperature range where $\tau_3$ is decreasing.

Besides the pressure-induced growth of the free volume in the bubbles, the increase of $\tau_3$ in niobium above 1100 K could be related to

(i) the desorption of helium, which eventually will segregate at grain boundaries,
(ii) the segregation of interstitial oxygen at the surface of the bubbles.

Possibility (i) is ruled out by the results on helium-irradiated molybdenum [35], where up to annealing temperatures of 1600 K no increase of $\tau_3$ is observed, and by helium outgassing experiments in molybdenum [40], where helium desorption from large bubbles was observed to start at 1900 K. If this temperature is scaled according to the melting temperatures of niobium and molybdenum, the onset of helium desorption from large bubbles in niobium is expected at 1600 K.

As far as possibility (ii) is concerned, it is interesting to inspect the correlation of $I_v$ and $\bar{\tau}$ (see figures 9 and 10) for the cases of helium-irradiated V and Nb. In helium-irradiated V (figure 9), $I_v(\bar{\tau})$ is a straight line parallel to the one for the deformed specimens. This behaviour of $I_v(\bar{\tau})$ indicates that the recovery in both cases is dominated by the disappearance of dislocations. In niobium, on the other hand, the recovery in the helium-irradiated and in the deformed specimens differs distinctly. The most prominent features in the case of the helium-irradiated specimens are the rapid initial recovery of the $I_v$ parameter which is accompanied by an increase of $\bar{\tau}$ and the absence of the stage 2 behaviour which is observed in the deformed sample and which was related to the uptake of oxygen in section 3.2.3. Between 900 K and 1255 K the correlation for the helium-irradiated samples is once more a straight line, including the reference point for the annealed sample. Again, this behaviour indicates the dominant recovery of a single defect type which is the large cluster, as may also be seen from figure 14. Most probably, the effects of oxygen resorption are suppressed in the helium-irradiated niobium because the initial defect concentration exceeds by an order of magnitude the concentration in the deformed sample and because these defects are initially stabilized by helium decoration. Thus a larger fraction of the oxygen impurities can permanently be trapped in large vacancy clusters close to the surface. The small fraction, which diffuses deeper into the volume of the specimen, will be distributed over considerably more defect sites and therefore the influence on the annihilation characteristics of the positrons will be further diminished.

A comparable study was only performed for niobium, irradiated at a temperature of 425 K with helium up to a concentration of 130 ppm [10]. The results are in disagreement with the present data, most probably because the samples used in [10] contained about 5000 ppm impurities. Thus the evolution of the defects in this case is most probably not dominated by the helium content but at least partially by other impurities.

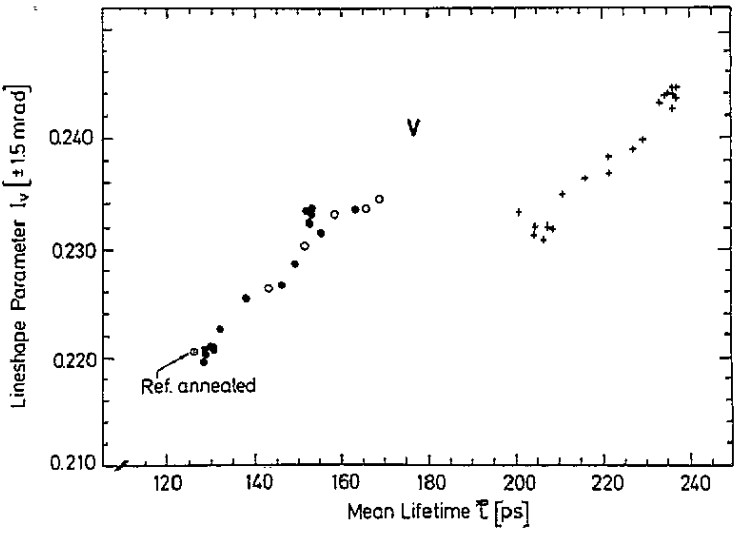


**Figure 9.** Correlation of the lineshape parameter $I_v$ and the mean lifetime $\bar{\tau}$ for vanadium at various states. The open circles are derived from the measurements at different deformations (see section 3.1). The full circles are taken from the annealing measurements of the deformed specimen; the crosses are derived from the annealing measurements of the $\alpha$-irradiated samples (see section 3.4). The reference value of the well-annealed vanadium is marked.

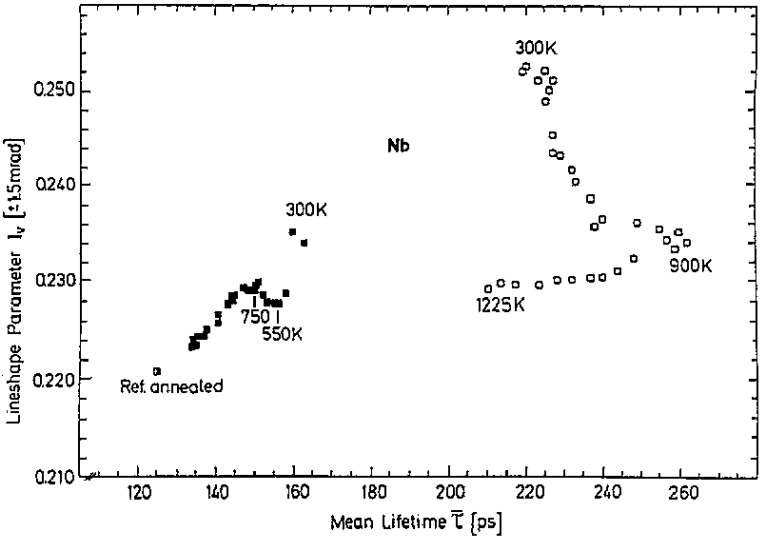


**Figure 10.** Correlation of the lineshape parameter $I_v$ and the mean lifetime $\bar{\tau}$ for deformed and $\alpha$-irradiated niobium at various annealing states. The full squares are derived from the annealing measurements of the deformed specimen; the open squares are derived from the annealing measurements of the $\alpha$-irradiated niobium. Some of the annealing temperatures are noted.

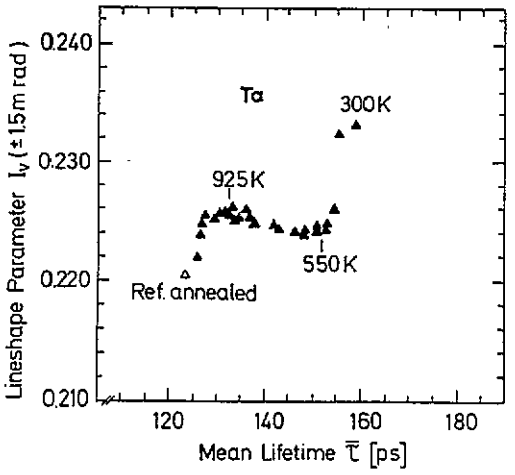


**Figure 11.** Correlation of the lineshape parameter $I_v$ and the mean lifetime $\bar{\tau}$ for deformed tantalum at various annealing states. Some of the annealing temperatures are noted.

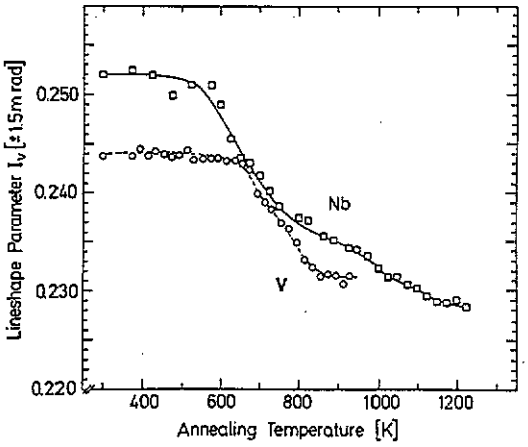


**Figure 12.** Lineshape parameter $I_v$ for helium-irradiated vanadium and niobium as function of the annealing temperature. The curves are only to guide the eye.

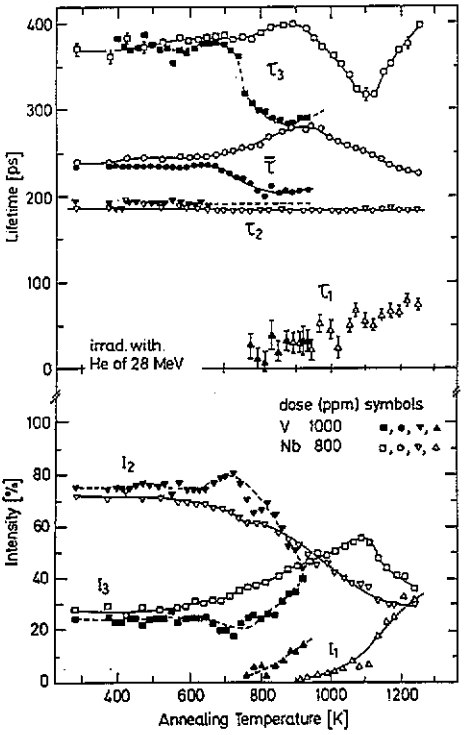


**Figure 13.** Lifetimes $\tau$ (upper part) and corresponding intensities $I$ (lower part) for helium-irradiated vanadium and niobium as function of the annealing temperature. The irradiation dose and the different symbols are given in the figure. The connecting curves are only to guide the eye.

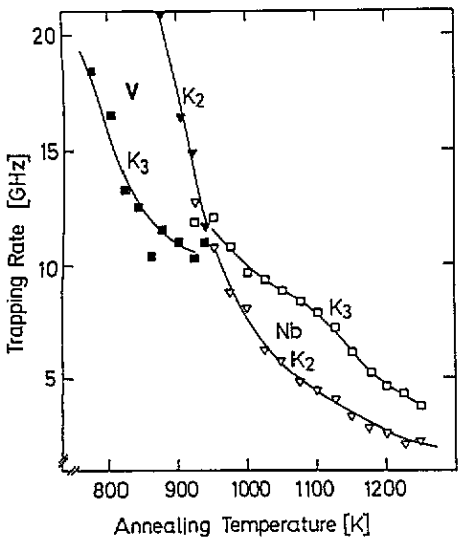


**Figure 14.** Calculated trapping rates $K$ for trapping at smaller ($K_2$) and larger ($K_3$) defects for helium-irradiated vanadium (full symbols) and niobium (open symbols) as function of the annealing temperature.

## 4. Conclusion

The annihilation characteristics of positrons and the recovery by thermal annealing of various kinds of defects in vanadium, niobium and tantalum were investigated. The following conclusions have been drawn.

(i) After deformation, in all three metals a single well-defined defect lifetime is observed which is 30 to 40 ps lower than that reported for vacancies. Thus in these BCC metals the trapping centres at dislocations must have a smaller free volume than vacancies.

(ii) The complete recovery of deformation-induced defects occurs in vanadium in a single stage within an annealing temperature range from 400 K to 550 K with a very good correlation of the average lifetime $\bar{\tau}$ and the lineshape parameter $I_v$ (see figure 9). In contrast to this, the recovery of the deformation-induced defects in niobium and tantalum is not completed even at an annealing temperature of 1200 K. Furthermore, in these metals large differences between the evolution of $\bar{\tau}$ and $I_v$ as a function of the annealing temperature are observed. These features are correlated with the uptake and with the diffusion of oxygen impurities at elevated temperatures.

(iii) In helium-irradiated vanadium and niobium, two distinctly different defect types are observed with characteristic lifetimes of about 190 ps and 375 ps. For the shorter lifetime $\tau_2$ and its related intensity $I_2$ a similar behaviour under isochronal annealing as in the case of the deformed specimens is observed. The other defect species is identified as large helium bubbles with an estimated helium density of 0.9 helium atoms per missing metal atom. A similar evolution of $\tau_3$ and $I_3$ is observed for both metals in the annealing study where $\tau_3$ decreases to a value of about 300 ps in a well-defined annealing stage and increases again at higher annealing temperatures. For niobium, both processes occur at a temperature which is about 200 K higher than in vanadium. The initial decrease of $\tau_3$ is attributed to the uptake of helium which is released from the smaller defects. By this process the internal pressure in the bubbles increases until the mechanical stability limit of the bubbles is reached. The subsequent increase of $\tau_3$ is attributed to the pressure induced growth of the free bubble volume.

(iv) All measured lifetime data are consistent with the simple trapping model.

## Acknowledgments

H Schröder is gratefully acknowledged for carrying out the irradiations with helium at the Forschungszentrum Jülich. The entire work benefited greatly from stimulating discussions with R Lässer.

## References

[1] Diercks D R and Loomis B A 1986 *J. Nucl. Mater.* **141–3** 1117
[2] Smith D L 1981 *J. Nucl. Mater.* **103, 104** 19
[3] Triftshäuser W 1986 *(Microscopic Methods in Metals) (Springer Topics in Current Physics 40)* ed U Gonser (Berlin: Springer) p 249
[4] Bentzon M D and Evans J H 1990 *J. Phys.: Condens. Matter* **2** 10165, and references therein
[5] Schaefer H E 1982 *Positron Annihilation* ed P G Coleman, S C Sharma and L M Diana (Amsterdam: North-Holland) p 369
[6] Trumpy G 1989 *Positron Annihilation* ed L Dorikens-Vanpraet, M Dorikens and D Segers (Singapore: World Scientific) p 431
[7] Maier K, Peo M, Saile B, Schäfer H E and Seeger A 1979 *Phil. Mag.* A **40** 701
[8] Mantl S and Singru R M 1979 *Phys. Rev.* B **19** 1391
[9] Hautojärvi P, Huomo H, Puska M and Vehanen A 1985 *Phys. Rev.* B **32** 4326
[10] Naidu S V, Sen Gupta A and Sen P 1987 *J. Nucl. Mater.* **148** 86
[11] Nambissan P M G and Sen P 1989 *Phys. Lett.* A **137** 149
[12] Hood G M and Schultz R J 1981 *J. Nucl. Mater.* **96** 15
[13] Gupta R P and Siegel R 1980 *J. Phys. F: Met. Phys.* L **7** 10
[14] Kögel G, Sperr P, Lässer R and Triftshäuser W 1993 submitted
[15] Suzuki H 1979 *Dislocations in Solids* vol 4, ed F R N Nabarro (Amsterdam: North-Holland) p 193
[16] Sestak P and Seeger A 1978 *Z. Metall.* **69** 195, 355, 425
[17] Hautojärvi P, Huomo H, Vehanen A and Plazaola F 1985 *Positron Annihilation* ed P C Jain, R M Singru and K P Gopinathan (Singapore: World Scientific) p 518
[18] Viswanathan B, Triftshäuser W and Kögel G 1983 *Rad. Effects* **78** 231
[19] Kirkegaard P and Eldrup M 1972 *Comput. Phys. Commun.* **3** 240
[20] Triftshäuser W 1975 *Festkörperprobleme (Advances in Solid State Physics)* vol XV, ed H J Queisser (Braunschweig: Pergamon/Vieweg) p 381
[21] Tanigawa S, Shinta I and Iriyama H 1982 *Positron Annihilation* ed P G Coleman, S C Sharma and L M Diana (Amsterdam: North-Holland) p 401
[22] Van Brabander F, Segers D, Dorikens M and Dorikens-Vanpraet L 1982 *Positron Annihilation* ed P G Coleman, S C Sharma and L M Diana (Amsterdam: North-Holland) p 472
[23] Noguchi M, Mitsuhashi T, Chiba T, Tanaka T and Tsuda N 1972 *J. Phys. Soc. Japan* **32** 1242
[24] Hörz G and Fromm E 1976 *Gase und Kohlenstoff in Metallen* ed E Fromm and E Gebhardt (Berlin: Springer) p 441
[25] Sanz J M and Hofmann S 1983 *J. Less Common Met.* **92** 317
[26] Halbritter J 1988 *J. Less Common Met.* **139** 133
[27] Palacio C and Martinez-Duarte J M 1982 *Thin Solid Films* **90** 63
[28] Legma B, Simon D, Bajard M T and Bardolle J 1983 *J. Less Common Met.* **95** 25
[29] Oechsner H, Giber J, Füßer H J and Darlinski A 1985 *Thin Solid Films* **124** 199
[30] Häkkinen H, Mäkinen S and Maninen M 1990 *Phys. Rev.* B **41** 12441
[31] Hasegawa M, Berko S and Kuramoto E 1989 *Positron Annihilation* ed L Dorikens-Vanpraet, M Dorikens and D Segers (Singapore: World Scientific) p 73
[32] Goodhew P J and Tyler S K 1981 *Proc. R. Soc.* A **377** 151
[33] Linderoth S 1989 *J. Phys.: Condens. Matter* **1** SA55
[34] Amarendra G, Viswanathan B, Bharathi A and Gopinathan G 1992 *Phys. Rev.* B **45** 10231
[35] Nambissan P M G, Sen P and Viswanathan B 1991 *Rad. Eff. Def. Solids* **116** 125
[36] Eldrup M 1992 *Mater. Sci. Forum* **105–110** 229
[37] Jensen K O, Eldrup M, Singh B N and Victoria M 1988 *J. Phys. F: Met. Phys.* **18** 1069
[38] Jensen K O and Nieminen R M 1987 *Phys. Rev.* B **36** 8219
[39] Trinkaus H 1983 *Rad. Eff.* **78** 189

[40] van Veen A, Evans J H, Buters W Th M and Caspers L M 1983 *Rad. Eff.* **78** 53
[41] Kobayashi N 1984 *J. Phys. Soc. Japan* **53** 3018
[42] Kögel G 1989 *Positron Annihilation* ed L Dorikens-Vanpraet, M Dorikens and D Segers (Singapore: World Scientific) p 52
[43] Hearmon R F S 1979 *Landolt–Börnstein, New Series* vol 11 (Berlin: Springer) p 114
[44] Vassen R, Trinkaus H and Jung P 1991 *Phys. Rev.* B **44** 4206
[45] Phitian J, Eyre B L and Bacon D J 1988 *J. Nucl. Mater.* **155–8** 1274
[46] MRC, Materials Research Company Ltd, UK
[47] Schaefer H E 1981 *Habilitationsschrift* Fakultät Physik, Universität Stuttgart p 124
[48] Hasegawa M, Kuramoto E, Kitajima K, Hirabayashi M, Ito Y, Takeyama T, Takahashi H and Ohnuki S 1982 *Positron Annihilation* ed P G Coleman, S C Sharma and L M Diana (Amsterdam: North-Holland) p 425